This is a repository copy of *Spontaneous formation of multilamellar vesicles from aqueous micellar solutions of sodium linear alkylbenzene sulfonate (NaLAS)*.

White Rose Research Online URL for this paper:
http://eprints.whiterose.ac.uk/158295/

Version: Accepted Version

Spontaneous formation of multilamellar vesicles from aqueous micellar solutions of sodium linear alkylbenzene sulfonate (NaLAS)

Sepideh Khodaparast[a],[*], William Sharratt[a], Haoyu Wang[a], Eric S. J. Robles[b], Robert Dalgliesh[c], João T. Cabral[a],[**]

[a]*Chemical Engineering Department, Imperial College London, SW7 2AZ London, United Kingdom*
[b]*The Procter & Gamble Company, Newcastle Innovation Centre, NE12 9TS Newcastle-Upon-Tyne, United Kingdom.*
[c]*ISIS Neutron and Muon Source, Science and Technology Facilities Council, Rutherford Appleton Laboratory, OX11 0QX Didcot, United Kingdom*

Abstract

We report the spontaneous formation of multilamellar vesicles (MLVs) from low concentration (< 30 wt%) aqueous micellar solutions of sodium linear alkylbenezene sulfonate (NaLAS) upon cooling, employing a combination of optical microscopy (OM), Small Angle Neutron Scattering (SANS), and Cryo-TEM. Upon cooling, MLVs grow from, and coexist with, the surfactant micelles, attaining diameters ranging from hundreds of nanometers to a few micrometers depending on the cooling rate, whilst the d-spacing of internal lamellae remains unchanged, at $\simeq 3$ nm. While microscale fluid and flow properties of the mixed MLVs and micellar phase depend on rate of cooling, the corresponding nanoscale structure of the surfactant aggregates, resolved by time-resolved SANS, remains unchanged. Our data indicate that the mixed MLV and micellar phases are in thermodynamic equilibrium with a fixed relative volume fraction determined by temperature and total surfactant concentration. Under flow, MLVs aggregate and consequently migrate away from the channel walls, thus reduce the overall hydrodynamic resistance. Our findings demonstrate that the molecular and

[*]Corresponding author
[**]Corresponding author
Email addresses: `s.khodaparast@imperial.ac.uk` (Sepideh Khodaparast), `j.cabral@imperial.ac.uk` (João T. Cabral)

mesoscopic structure of ubiquitous, low concentration NaLAS solutions, and in turn their flow properties, are dramatically influenced by temperature variation about ambient conditions.

1. Introduction

Surfactants are the key components of commonly used detergents and numerous household products. [1, 2] Among these, anionic surfactants and especially the commercially significant biodegradable linear alkylbenzene sulfonates (LAS)
5 comprise up to 30% of the total weight of the household cleaners. [3, 4] LAS exhibits a rich phase behaviour with distinct bulk properties, such as viscosity and optical transparency, associated with various self-assembled phases. [5] Although the location of the boundaries between the different phases of LAS is system-specific, the transformation pathways between the different phases are
10 shared by many other chemical and biological systems. [6, 7, 8, 9, 10, 11, 12]

Previous investigations of the phase behaviour of LAS were mainly dedicated to higher concentrations ($>$ 30 wt%), for which a densely packed planar lamellar phase L_α coexists with a micellar phase L_1 at room temperature. [13, 14, 15] For intermediate LAS concentrations (40 to 60 wt%), a nearly composition-
15 independent line in the phase diagram, around 50°C, defines the boundary between an opaque planar lamellar phase (L_α in Fig. 1) with a uniform d-spacing ($32-34$ Å), and a semi-transparent lamellar phase (L'_α in Fig. 1). The d-spacing of the L'_α phase was found to significantly increase upon heating the solution, especially at lower LAS concentrations (up to around 44 Å at 35 wt% of LAS).
20 [14]

Applying shear stress or addition of salt to the planar lamellar phase of anionic surfactants, such as LAS, is known to promote the bending and wrapping of the bilayers, and thus transform them into multilamellar vesicles (MLVs). [16, 17, 18, 15] These onion-like liquid crystalline droplets typically have diam-

eters ranging from tens of nanometers to a few micrometers.[19, 20, 21, 22, 23] The MLVs formed under shear are not, however, thermodynamically stable and revert to the original equilibrium planar lamellar phase in the absence of shear. To the best of our knowledge no report of spontaneous formation of vesicles in LAS systems is available in the literature. MLVs were mainly found to form spontaneously from the micellar phase in catanionic and zwitterionic surfactant solutions. [24, 25, 26, 27, 28]

Despite decades of research into phase behaviour of LAS and its numerous industrial applications, fundamental understanding of LAS phase behaviour at lower concentrations and temperatures remains elusive. At such concentrations (< 30 wt%), the behaviour of aqueous solutions of LAS is estimated by extrapolation of the trends from solutions of higher concentration. [13] However, physical and functional properties of LAS solutions in this regime were observed to be significantly different from those expected from the characterised micellar and lamellar phases described before. [29, 30] In particular, Pommella *et al.* recently reported complex rheological and flow behaviour for aqueous solutions of 30 wt% LAS at 25 °C. The non-planar lamellar nano-structure of the surfactant solution under these conditions, which induced such flow behaviour, was assumed to be generated by the shear applied during the sample preparation.[30] Here, we show that the significant change in the macroscopic and flow behaviour of LAS solutions derives from the spontaneous surfactant self-assembly into non-planar bilayers, as opposed to shear-driven deformations. To investigate this spontaneous transformation and its potential impact on the physical properties of LAS solutions, we study the phase behaviour of LAS at weight concentrations below 30 wt% in deionised water and temperatures ranging between 0 to 40 °C, as illustrated in Fig. 1. LAS is used in its common neutralised form here, thus being referred to as sodium alkylbenzene sulphonate NaLAS from here on.

We employ bright-field and cross-polarised optical microscopy to detect the phase transitions in aqueous micellar solutions of NaLAS at mesoscale, upon cooling at controlled rates. Using a combination of Small Angle Neutron Scat-

tering (SANS) and Cryogenic Transmission Electron Microscopy (Cryo-TEM), we resolve the nanoscale structure of NaLAS phases under similar environmental conditions. Finally, we examine the behaviour of NaLAS solutions under well-defined hydrodynamic stress, using a microfluidic approach. Our goal is to elucidate the phase transformations of NaLAS solutions across lengthscales and exploit this knowledge to rationalise their complex flow behaviour.

2. Materials and Methods

Linear sodium alkylbenzene sulfonate was provided by Procter & Gamble as a 45 wt% concentrate. A large volume of this solution (0.5 L) was heated at 75 °C for 4 hours and homogenised regularly before sequentially preparing the dilutions in deionised water (CENTRA, ELGA LabWater). The NaLAS sample used here is a mixture of alkyl chains of C_{11} to C_{14} and different phenyl isomers (2- to 7-phenyl), as described in an earlier work. [15]

2.1. Quiescent measurements

Optical microscopy. Quiescent experiments (i.e., in the absence of flow) were performed by placing a 3 μL droplet between two round cover slips of 19 mm diameter, thus providing a uniform sample thickness of approximately 10 μm. Linear cooling profiles were applied using a thermal stage (Linkam, LTS420) with rates ranging from 0.05 °C/min to 50 °C/min. Isothermal measurements were performed by quenching the sample at $\alpha_c = 50$ °C/min to the final temperature T_f and maintaining the final temperature T_f with an accuracy of 0.1 °C. Both polarised and bright-field microscopy images were captured with an Olympus BX41M-LED microscope, using a 50X objective (Olympus, MPlanFL with NA 0.75) and a CMOS camera (Basler ace ac2040-90 uc), which provided an overall spatial resolution of 0.3 μm per pixel. Bright-field microscopy images were used to determine the phase boundaries. Images were recorded at the rate of 1 frame per second, whilst the temperature was linearly decreased at the rate of $\alpha_c = 0.05$ °C/min. The phase transition temperature

4

T_c was defined as the point at which the relative difference of the average light intensity between two consecutive images in a cooling sequence first reached 2% (Fig. S1).

SANS measurements. In SANS experiments, the 45 wt % NaLAS aqueous solution (in H_2O) was diluted in D_2O to reach the desired lower concentrations. Isothermal and linear cooling rate SANS experiments were carried out on the D22 diffractometer (ILL, Grenoble, France) in quartz cells (1 mm banjo, Hellma) with incident neutron wavelength $\lambda = 6$ Å and $\Delta\lambda/\lambda = 10\%$. Isothermal measurements were performed at sample-to-detector distances of 1.4, 5 and 17 m yielding a Q-range of 0.0028-0.6 Å^{-1}, whilst the resolved cooling measurements were carried out at a fixed detector distance of 5 m, yielding a Q-range of 0.01-0.17 Å^{-1}. Temperature control was achieved by circulating baths connected to the sample rack (F4-K, Haake) and measured with a PT100 probe inserted into the rack, next to the sample of interest.

Time resolved SANS experiments at fixed heating and cooling rates (ranging from 0.5 to 50 °C/min) were performed on the LARMOR diffractometer (ISIS, pulsed neutron source, UK), with a polychromatic λ=0.9-13.3 Å beam with sample-to-detector distance = 4.1 m, yielding $0.005 \lesssim Q \lesssim 0.3$ Å^{-1}. Data acquisition was carried out in 'event mode' enabling optimal time-slicing of the data a posteri. A custom-made cell holder and a thermal stage (Linkam) were used to control of heating/cooling rate during SANS measurements. SANS data from D22 were reduced with GRASP (V7.15CD), corrected by the empty cell and electronic background before intensity calibration to absolute units (cm^{-1}) by the direct beam flux. IGOR Pro (V6.37) was used to stitch isothermal measurements at different detector distances, using the NIST SANS reduction macros. The SANS data from LARMOR were reduced, using standard procedures in MANTID.[31] Data from both D22 and LARMOR were fitted in SASView (V4.1.2).

Cryo-TEM measurements. To prepare the vitrified samples for Cryo-TEM, 3 μl of the sample was placed on a copper TEM grid covered by a perforated carbon film in a controlled environment vitrification system (Vitrobot) at

5

the desired subcooled temperature and humidity. The grid was plasma treated beforehand to increase its surface hydrophilicity and thus ensure the spreading of the sample. The excess solution was removed by blotting with filter paper, after which the sample was immediately plunged into liquid ethane. Finally, the specimens were stored in liquid nitrogen and examined with a Tecnai T12 TEM at 120 kV and images were captured by a CCD camera (TVIPS, TemCam-F216).

2.2. Microscopic flow analysis

Flow behaviour of NaLAS solutions were investigated in microchannels fabricated in polydimethylsiloxane (PDMS) using conventional soft lithography. [32] The open microchannels (width $\times$ height $= 6000 \times 60 \ \mu\text{m}^2$) were bonded to a glass cover slip that was brought in contact with the thermal stage to create a thermal boundary similar to that of the quiescent measurements. Shallow and wide microchannels were chosen here in order to increase the area exposed to the temperature control stage and minimize the temperature non-uniformities across the depth of the channel. NaLAS solutions were injected into the channels at constant flow rates using a syringe pump (Harvard Apparatus, 33 DDS). Pressure was measured at the inlet of the channel using a microfluidic inline pressure sensor (Elveflow, MFP), while the outlet was kept at atmospheric pressure. Flow visualisation was performed in both bright-field and cross-polarised settings, as described before.

3. Results and discussion

3.1. Phase behaviour

The phase behaviour of aqueous NaLAS solutions has been previously studied at relatively higher concentrations (> 30 wt%) and temperatures (20-90 °C). [13, 14] A broad two-phase region with coexisting micellar L_1 and lamellar L_α phases was reported for the range of 30 to 60 wt% NaLAS concentration, see Fig. 1. In this region, a nearly concentration-independent phase boundary was found to separate a tightly packed optically opaque mixed lamellar phase

6

(L_1+L_α) with d-spacing around $32 - 34$ Å at lower temperatures ($T < 40$ °C) from a translucent lamellar phase referred to as L'_α. The latter was characterised

by a varying d-spacing with temperature and NaLAS concentration. In this work, we measure for the first time the phase boundaries in the 5-30% NaLAS concentration range and 0-40 °C temperature range, reporting nano- and microscale solution behaviour, as depicted in Fig. 2. The observed boundaries are slightly offset (by approximately 5% NaLAS towards lower concentrations)

from a previously reported extrapolated boundary. [13] This is unsurprising given the uncertainties associated with extrapolation, the different experimental methods, and variation of isomeric and chain length distributions between surfactant batches and grades.

Our optical microscopy measurements reveal round birefringent droplets of

lamellar phase (termed L_α) with symmetric Maltese crosses, formed from the optically transparent isotropic micellar L_1 solution of NaLAS upon cooling, see Fig. 2. The phase boundary depicts the temperature at which the initial formation of droplets is observed in OM measurements, when cooling the samples at very low rates ($\alpha_c < 0.5$ °C/min). The growth rate of the droplets was found

to depend on the rate of cooling, however, the temperature at which the phase separation first occurs remains unchanged for sufficiently small cooling rates (Fig. S2).

SANS measurements show distinctive scattering patterns for conditions below and above the phase boundary, in agreement with OM results. The spon-

taneous formation of lamellar droplets is accompanied by the appearance of a sharp Bragg peak at high-Q, and an upturn at low-Q in the SANS profile (Fig. 2, bottom right/left). The SANS measurements confirm the coexistence of the micellar L_1 (peak at intermediate-Q) and the lamellar L_α (at low-Q and high-Q) phases below the phase boundary. With the lowest accessible Q-values in our

experiments, no plateau in the scattering intensity was observed in the low-Q region and therefore determination of the aggregate size could not be resolved. However, evidence from OM and SANS measurements indicate the formation of multilamellar vesicles (MLVs), further confirmed by electron microscopy which

reveals the internal structure of MLVs. Therefore, in this work, L_α refers to the lamellar phase in the form of MLVs from here on, unless otherwise indicated.

For concentrations below 10 wt%, the solution remains in the micellar phase and no transition to the lamellar phase is found upon cooling down to 0°C, whilst above 30 wt% NaLAS concentration, the system exhibits coexistence of MLVs and bulk lamellar and micellar phases (Fig. 1).

3.2. Formation of MLVs from micellar phase

The symmetric Maltese cross patterns found within the droplets (Fig. 2) are characteristic of the formation of concentric multilayer lamellar MLVs.[12] This is further confirmed by our Cryo-TEM measurements, which resolve the internal structure of MLVs, as shown in Fig. 3.

The low-Q upturn and the high-Q Bragg peak in the isothermal SANS profiles for 15 and 20 wt% of NaLAS in Fig. 3 correspond to Porod scattering from the large droplets and the regular repeating spacing between bilayers of surfactant molecules in the lamellar phase, respectively. At a similar temperature ($T = 5.6$ °C), only a micellar phase with a peak at intermediate-Q is found for lower concentrations (5 wt%). The d-spacing of the lamellar structure found in the TEM measurements agrees favorably with that obtained from the SANS data and remains unchanged for the range of concentrations and temperatures tested here, 30.2 ± 0.2 Å. This value also agrees well with the d-spacing found for MLVs formed upon shearing and addition of salts to solutions of NaLAS at higher concentrations (> 45 wt%). [15]

Similarly, continuous cooling of the solutions at lower rates ($\alpha_c \approx 0.1$ °C/min) shows simultaneous growth of micro-scale liquid droplets and formation of lamellar structures below the phase transition temperature T_c, for a fixed concentration of NaLAS (Fig. 4a). Alongside the appearance of the high-Q Bragg peak of the lamellar phase, the intensity of the micellar peak in the scattering profile continuously decreases, whilst its location moves towards lower values of Q, as expected for a decrease in micellar concentration, see the inset in Fig. 4a. Next, we track the scattering intensity at $Q = 0.01$ Å^{-1} and $Q = 0.2$ Å^{-1}, that

8

correspond to the larger scale compact shape of the MLVs and their internal

²⁰⁵ lamellar structures, respectively. Fig. 4b shows that the initial appearance and the growth of these two structures occur simultaneously, within the temporal resolution of our SANS experiments. Moreover, the temperature at which the initial growth of both structures is observed in the SANS profiles coincides with the corresponding phase transition temperature detected by optical microscopy.

²¹⁰ *3.3. SANS data analysis*

The total scattered intensity obtained in SANS measurements at temperatures below the phase boundary $(L_1 + L_\alpha)$ can be decomposed into two major contributions: (1) micelles at intermediate-Q range (0.01 Å^{-1} $< Q < 0.3$ Å^{-1}), and (2) MLVs at low-Q ($Q < 0.01$ Å^{-1}) and high-Q ranges (0.18 Å^{-1} $< Q <$

²¹⁵ 0.01 Å^{-1}), see Fig. 5a. The micellar contribution is fitted using an ellipsoidal core-shell model for the form factor and the Hayter-Penfold rescaled mean spherical approximation (RMSA) to model the structure factor. Although RMSA was originally developed for spherical particles, it has been shown to hold for ellipsoidal particles with relatively larger inter-micellar distance. [33] The fit to the

²²⁰ scattering pattern from the micelles presented in Fig. 5a yields an equatorial core radius of 12 Å, shell thickness of 5 Å and average core radii ratio of 2.8, corresponding to a prolate ellipsoid. The best micellar fit is obtained using scattering length densities SLD$_{core}$ = -0.46 $\times 10^{-6}$ Å^{-2} and SLD$_{shell}$ = 1.69 $\times 10^{-6}$ Å^{-2}. These fitted values are consistent with our estimation of SLDs based on

²²⁵ geometric calculations, considering sodium benzenesulfonate as the shell and an average of 12 carbons in the alkyl chain as the core. Details of these estimations are provided in Supporting Information, Section 3. The fitted micellar charge remains approximately unchanged (at about 19 e^-) for concentrations tested here. The ellipsoidal core-shell model was found to provide a satisfactory

²³⁰ fit to our scattering data at different concentrations and temperatures, while model fits to polydisperse spherical micelles consistently provided poorer agreement with the experimental data. At all concentrations of NaLAS tested here, the volume fraction of micellar phase estimated through this fitting procedure

closely follows the volume fraction of the surfactant in the mixture considering the density of the NaLAS, thus suggesting that majority of surfactant molecules participate in the formation of micellar aggregates, see Fig. S4.

The lamellar signal is well described by a power law $I(Q) \sim Q^{-4}$ compatible with polydisperse densely packed sharp droplets ($\bar{d} > 100$ nm) at low-Q [34] and a Gaussian distribution around the Bragg peak associated with the bilayer structures at high-Q. The Gaussian curve is fitted to the scattering intensity in the corresponding Q range, after subtracting the fitted micellar contribution $I(Q)_{\text{tot}} - I(Q)_{L_1}$, as shown in Fig. 5b,c. At any given temperature and concentration the complete fit to the SANS profile is obtained by summation of these contributions, as illustrated in Fig. 5b.

Upon continuous cooling of the sample, the Gaussian fit to the lamellar contribution of the scattered intensity is found to remain centered around a fixed wavevector Q^* corresponding to a d-spacing= 30.2 ± 0.2 Å, whilst its maximum intensity increases as the fraction of MLVs increases at the expense of surfactant micelles in the solution (Fig. 5c,d). Below the corresponding phase transition temperature ($T_c \approx 8\ ^\circ$C), the contributions of the lamellar structures at high-Q exhibit a shape-invariant Gaussian profile when normalized by the maximum scattered intensity I_{max} obtained at Q^*, as illustrated in Fig. 5c.

3.4. Growth and dissolution of the MLVs

Cooling. In order to characterise the microscopic growth of MLVs, a series of cooling and heating ramps were imposed on 15 wt% NaLAS solutions under quiescent conditions. Upon continuous linear cooling, the final diameter of the MLVs and their growth rate were found to be controlled by the rate of cooling α_c (Fig. 6a). This process appears well described by a nucleation and growth mechanism. At lower rates of cooling ($\alpha_c < 1\ ^\circ$C/min) a limited number of nucleation sites are present and droplets slowly ($< 0.1\ \mu$m/s) grow up to 10 μm in diameter until they reach the limited thickness of the sample in our experiments ($t \approx 10\ \mu$m). Consequently, the optical detection of the phase separation in its initial stages is not possible under these conditions, as the bulk sample remains

10

transparent due to the small number density and the low growth rate of the droplets. In contrast, at higher rates of cooling ($\alpha_c > 1$ °C/min), the number density of MLVs significantly increases relative to the former case, whilst the diameter of the droplets remains smaller than 5 μm. In such a condition, the larger number density and higher growth rate of the droplets, leads to turbidity that is clearly visible by the naked eye.

Droplet diameter and area coverage obtained by OM during linear cooling ramps are reported in Fig. 6b. At low rates of cooling, droplets grow slowly into a 'pancake' shape in our thin sample setup, and consequently the area coverage measured by OM closely represents the volumetric concentration of the MLVs ($\phi \approx A\%$). At higher rates of cooling, where droplets are smaller and not deformed by the confinement, the apparent area coverage measured by OM largely overestimates the volumetric concentration of the MLVs, due to the finite visibility depth of the approach. Therefore, we expect quantitative agreement between SANS and OM data only at lower rates of cooling, for which the OM projected area reflects MLV concentration.

Heating. Two distinct trends were found during the heating cycle at a fixed rate ($\alpha_h = 1$ °C/min): (i) The number density of larger droplets (formed at low α_c) remained largely unchanged, while their size decreased over time; (ii) by contrast, the number density of smaller droplets decreased whilst the size of undissolved droplets remained approximately constant. Droplet formation appears fully reversible and the solution returns to homogeneity (micellar L_1) upon heating back to room temperature (Fig. 6a).

Similar to other nucleation and growth processes, the apparent phase transition temperature upon cooling decreases with increasing rate. [35] Likewise, as the heating rate increases, higher temperatures must be reached for complete dissolution of the droplets, resulting in a wider apparent metastable zone width (MSZW), see Fig. 6c. [36]

Thermal reversibility. In order to assess the reversibility of the micellar-to-MLV transformation, a series of thermal cycles and isothermal measurements were carried out by SANS, as shown in Fig. 7. We find that, regardless of ther-

11

mal pathway (*i.e.* cooling and heating profile) both the micellar and lamellar Bragg peak position and intensity remain unchanged, upon thermal equilibration over 30 minutes. As expected from the OM observations, the low-Q upturn associated with the MLV formation is impacted by thermal rate, albeit only slightly. Benefiting from the absolute calibration of the SANS data, we thus show that for a given concentration and temperature there is a well defined volume fraction of micellar and lamellar phase that coexist at equilibrium.

3.5. Micellar to lamellar phase transformation and coexistence

The maximum scattered intensity associated with the micellar contribution, accompanied by the increasing intensity of the Bragg peak, in our SANS measurements indicates the transformation of the micellar phase into MLVs (Fig. 8a). Assuming that the lamellar phase is formed from the micellar phase and considering a similar packing volume for the surfactant molecules, the volume of the lamellar phase can be roughly estimated by the loss of the volumetric concentration of the micellar phase calculated by fitting the SANS data in the two-phase region (Fig. S5).

Transformation pathways, including the formation of unilamellar vesicles have been investigated over the past two decades.[12] To form vesicles, micelles are typically expected to first grow into disk-like bilayers, that extend, fuse and bend to form closed unilamellar assemblies. [37] In such conditions, the topological fate of the lamellar phase depends on the balance between the unfavourable energy at the edge of the growing bilayer disks and the bending energy required to form spherical lamellar droplets. [38, 39, 11, 40, 41] Other proposed pathways involve initial elongation of the micelles into longer rod-like structures, that eventually develop into unilamellar or multilamellar vesicles. In our OM experiments, MLVs are observed to form in at least two distinct coexisting pathways: (1) Round sub-micron birefringent droplets appear spontaneously and grow gradually, exhibiting Maltese cross patterns from the beginning of the process, suggesting a multilamellar structure within the droplets. (2) Extended vesicles (100s μm) with thin lamellar shells are initially formed. These thin

12

structures then become the source for the formation of multiple MLVs growing from their shells until the entire body of the vesicle disappears. Within the time resolution of our isothermal SANS measurements, the exponent of the power law fitted to the low-Q range changes from $\beta \approx 0$ (micellar) to $\beta \approx -2$ (unilamellar vesicles) within the first few minutes of the experiments. This observation can be associated with the formation of relatively thin large vesicles. At longer times, the low-Q upturn increases further reaching $\beta \approx -4$, suggesting that the number of the bilayers within vesicles is increasing and the structures become more compact.[34] At even longer times, the coalescence of relatively monodisperse MLVs results in larger, transient polydisperse (in size and shape) aggregates, as observed by OM. This period is characterised by low Q power laws ranging from -2 to -4, which evolve non-monotonically over time, as shown in Fig. 8b. The transformation pathways suggested by our OM observations and SANS measurements are schematically illustrated in Fig. 8c.

3.6. MLVs under flow

Generally, the transformation of planar lamellar phase into MLVs was found to enhance the solution "flowability and firmness", in industrial parlance, whilst decreasing its adhesion to the boundaries of the transport conduits. [17] Recent rheology measurements of HLAS at concentrations and temperatures relevant to our range of interest, showed significant shear-thinning behaviour with multiple power-laws associated with different ranges of shear rate ranges.[30] This behaviour was attributed to the presence of MLVs that were assumed to form due to the application of shear to the planar lamellar phase.[30] Our quiescent experiments now show that MLVs form spontaneously within the micellar phase of NaLAS upon crossing the phase boundary. In order to investigate this spontaneous phase transformation upon cooling, we performed microfluidic experiments that model confinement effects, while allowing design of well-controlled complex shear fields and simultaneous visualisation of the flow.

Comparison between our OM and SANS measurements presented in Fig. 6, 7 and 8, suggest that despite the concentration equilibrium between the L_a and

13

L_α phase at a given temperature, microscale properties of the MLV phase are strongly influenced by their formation pathway, for instance the cooling profile. Therefore, we expect the flow properties of the MLV phase to be a complex function of shear stress, cooling rate, geometrical confinement relative to the size of the droplets and time. In order to isolate the effect of flow on the effective solution viscosity at different temperatures, we choose our experimental control parameters to avoid deformation of MLVs and consider quasi-isothermal conditions. We use a shallow (60 μm) and wide (6000 μm) geometry of the channel here to achieve a uniform temperature in the direction of the flow, as well as over the cross-section of the channel. Furthermore, the larger width of the channel compared to the typical diameter of the MLVs (up to 1-10 μm) ensures no significant deformation of the droplets due to geometric confinement. Based on estimations of the kinetics of the micellar-MLV transformations from our previous measurements presented in Fig. 6, we apply a well controlled temperature profile to the bottom wall of the microchannel (detailed in Fig. 9a, top) and a flow rate of 10 μL/min. These temperature limits allow all the tested samples of different concentrations (10, 15 and 20 wt%) to experience a phase transition from the micellar L_1 to the coexisting micellar/lamellar phase $L_1 + L_\alpha$. The residence time of the sample in the channel is typically around 50 seconds, thus the relatively low cooling rates (here $\alpha_c = 2$ °C/min) ensures that considering the fluid experiences a maximum temperature variation below 1.6 °C during its flowing time in the channel. This provides quasi-isothermal conditions, while allowing for a longer induction time t_i necessary for the formation of the MLVs at higher subcooled temperatures T_f, see Fig. S4 for measurements of T_i versus T_f. Lower rates of cooling are not employed since the appearance and growth of the MLVs are not homogeneous in the field and droplets grow to a size that is comparable to the dimensions of the channel, thus their deformation under flow becomes significance. For the current settings, the relative increase in the diameter of the MLVs during this residence time is less than 5%, therefore, droplets effectively maintain their size during cooling, whilst the sample temperature determines their number density. We use measurements of the pressure drop

14

ΔP for the flow of the surfactant solution at a constant rate ($Q = 10$ μl/min) in the channel as an indirect tool for quantifying the effective viscosity of the fluid and thus the "flowability" of the solution at different temperatures. Depending on the concentration of the solutions, three distinct trends of ΔP are found (Fig. 9a). The results are rescaled based on the smallest ΔP obtained for the purpose of comparison between the different concentrations.

At 10 wt% NaLAS, the changes in pressure drop during cooling are within measurement uncertainty. Upon reaching the phase transition temperature ($T_c = 5$ °C, see Fig. 2) a detectable jump is observed, which is reversed upon heating above this temperature. Under these conditions, the pressure drop profile tracks the phase transition temperatures. At higher concentrations, 15 wt%, the effective viscosity of the sample and consequently the pressure drop in the channel rise immediately upon cooling and largely follow the temperature profile. The effective viscosity profile exhibits a degree of asymmetry which we rationalise by the asymmetric kinetics of the growth and the dissolution of the MLVs. At even higher concentration, 20 wt%, the effective viscosity and the pressure drop appear non-monotonic in time, due to an interplay between high density MLV formation and migration under flow. We observe that ΔP initially increases with cooling from ① to near the phase boundary at ②, where it reaches a maximum associated to the formation of homogeneously distributed MLVs at high number density. These aggregate and thus migrate towards the center of the channel (with low shear stress), illustrated in Fig. 9b, thereby reducing the effective solution viscosity and overall pressure drop in ③. This behaviour is reminiscent of the Fåhræus-Lindqvist effects observed in blood flow in small capillaries, [42] in which red blood cells move away from the walls, towards regions of lower velocity gradient.[43] During heating, the aggregates first break apart and cause a relative increase in ΔP indicated by ④, followed by a gradual decrease, as isolated droplets dissolve back into solution, shown by ⑤, returning to the starting value of the cycle at 30 °C.

The pressure drop thus depends on multiple factors: concentration of the NaLAS solution, degree of sub-cooling, the flow rate and distribution of shear

stress in the flow. In the concentration and temperature range explored here, deeper subcooling has qualitatively similar effects to increasing sample concentration, since they both lead to higher rates of transformation from the micellar to MLV phase. In turn, this promotes formation of larger aggregates and their migration away from the channel wall. Our spatiotemporal visualisation of MLV formation under well-defined flow fields, rationalises the significance of phase behavior in affecting macroscopic properties of the NaLAS solutions, such as hydrodynamic resistance and adhesion to the solid boundaries of processing units.

4. Conclusions

We have mapped the phase behavior of the ubiquitous NaLAS water system in the low concentration (< 30 wt%) and temperature (0 to 40 °C) regime, hitherto unexplored. Here we report a spontaneous transition from the micellar phase to MLVs (in the absence of shear or salt addition) and comprehensively characterise the transformation with an array of complementary experimental techniques. In particular, we linked the microscale formation and growth of the MLVs obtained in OM to the internal molecular structure of the nanoscale self-assemblies obtained from Cryo-TEM and SANS, as well as their macroscopic flow properties. The observed boundaries between the L_1 and L_α in the range of concentrations and temperatures studied here are consistent, albeit slightly offset from reports that extrapolated the phase boundaries to this concentration range. [13] Upon cooling, we found micelles to gradually transform into multilamellar vesicles, whose size and number density in the solution strongly depend on the rate of cooling. Our measurements show that formation of MLVs result in significant reduction in micelle concentration, that may in turn influence the emulsification efficacy of the solution. Comparison between our OM and SANS measurements suggests that a well-defined equilibrium exists between the concentrations of the micellar and the lamellar phase at a given temperature. By contrast, the microscale properties of the MLV mixed phase are strongly influ-

16

enced by the rate of cooling. This finding motivates further investigations of the effect of cooling rate on the micro- and macroscopic behaviour of NaLAS or model systems comprising similar phase behaviour in the future. OM microscopy observations supported by SANS measurements suggest existence of vesicles with thin shells and compact multilamellar vesicles at different stages of the transformation from the micellar to the MLV phase. However, higher resolution in time is still required to fully elucidate the early stage of this process. When cooling under flow, formation of MLVs is clearly reflected in the overall pressure drop in the system, providing a potentially additional tool for mapping phase boundaries of the system. Moreover, in such a conditions MLVs were found to migrate away from the stationary walls of the microchannel, due to the non-uniform shear distribution in the cross-sectional plane. Therefore, the partial transformation from the micellar to MLV phase, along with the effect of non-uniform shear stress on the migration of the microscopic structures, becomes an important factor in defining their macroscopic flow behaviour.

Figure 1: Phase diagram of aqueous solution of NaLAS in the low concentration regime. Images correspond to bright-field (right side) and cross-polarised (bottom) micrographs of NaLAS solutions obtained by varying temperature and concentrations, respectively. At intermediate concentrations ($> 30\%$), a nearly concentration-independent [14] phase boundary separates an opaque lamellar phase L_α from a semi-transparent L'_α. The region of interest of this work is indicated by a dashed boundary in the phase diagram. Scale bar applies to all micrographs in the figure.

18
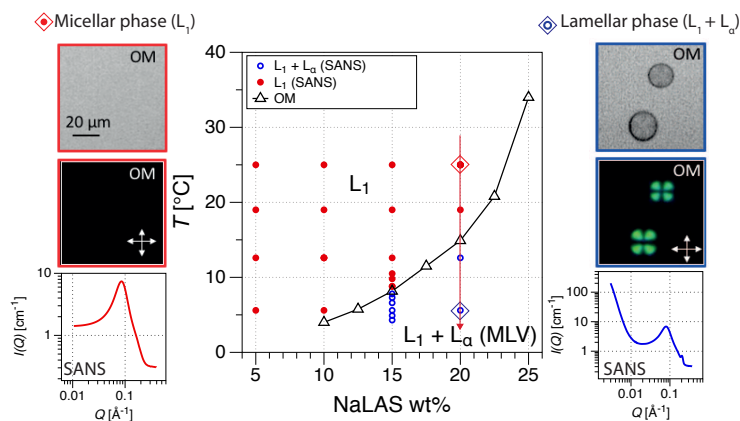
Figure 2: Phase diagram of aqueous solution of NaLAS at concentrations below 30 wt%. Open triangles are obtained by tracking the average light intensity of bright-field optical microscopy (OM), acquired while cooling the samples at the rate of $\alpha_c = 0.05$ °C/min. Closed and open circles correspond to the micellar L_1 and lamellar $L_1 + L_\alpha$ phases, respectively obtained in SANS measurements. Insets on the left and right side of the phase diagram correspond to measurements using bright-field (top), and cross-polarised microscopy (middle) and SANS (bottom), respectively. Crossing the phase boundary, birefringent spherical droplets of highly concentrated surfactants are formed within the solution, accompanied by an increase in forward scattering and the emergence of a sharp peak at $Q^* \approx 0.02$ Å^{-1} in SANS. Scale bar applies to all micrographs in the figure.

References

[1] D. Myers, Surfactant Science and Technology, Wiley, 2005.

[2] I. Johansson, P. Somasundaran, Handbook for Cleaning/Decontamination of Surfaces, Elsevier, 2007.

[3] A. E. Hargreaves, Chemical Formulation: An Overview of Surfactant-Based Preparations Used in Everyday Life, Roy. Soc. Chem., 2003.

[4] Global surfactants market 2018- segmented by origin, type, application, geography-grwoth, trends and forcasts to 2023 [online] (2018).

19
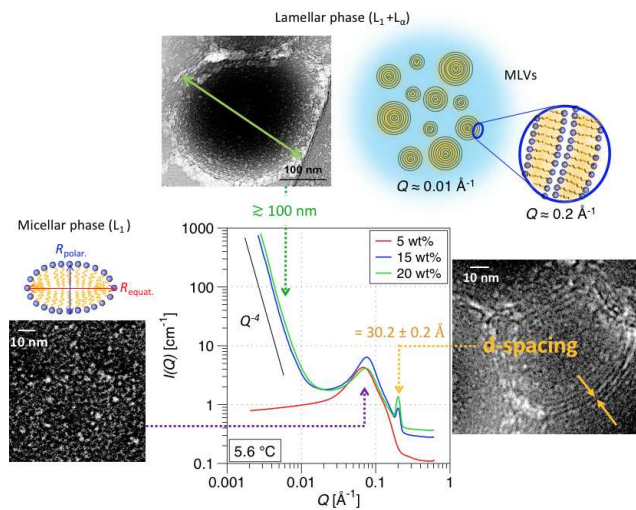
Figure 3: Self assembly of aqueous solution of NaLAS (below 30% weight concentration) from micellar phase L_1 and mixed $L_1 + L_\alpha$ lamellar phase, resolved by Cryo-TEM and SANS. At a given temperature (here shown at 5.6 °C), only the micellar phase exists at a lower concentration 5 % (red curve), whilst multilamellar vesicles MLVs coexist with the micellar phase at higher concentration 15, 20 wt% (blue and green curves). The formation of MLVs leads to the appearance of low-Q peak and high-Q upturn in the SANS scattering profile. The sharp Bragg peak at $Q \approx 0.2$ Å^{-1} corresponds to the d-spacing $= 30.2 \pm 0.2$ Å of the lamellar structure. The self-assembly of the lamellar structures into multilamellar vesicles is confirmed by Cryo-TEM, that quantitatively corroborates the d-spacing of the internal lamellar structure. The Q values indicated in schematics correspond to relevant length scales of MLVs and lamellar spacing.
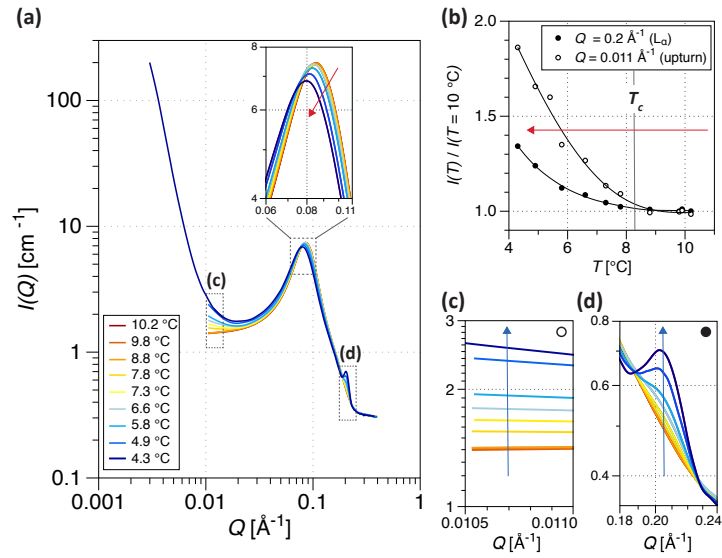
Figure 4: Formation of microscale MLVs from NaLAS micellar solution. (a) Radially averaged SANS data for an aqueous solution of 15 wt% of NaLAS at different temperatures, obtained by decreasing the temperature in 0.5 °C steps with a waiting time of 5 min. (b) Evolution of the scattering intensity at low-Q and high-Q ranges versus temperature. As the sample is cooled across the phase boundary, a simultaneous rise in the scattered intensity at low-Q (c) and high-Q (d) ranges is observed, associated with the microscale droplet formation and the nanoscale lamellar structure, respectively.
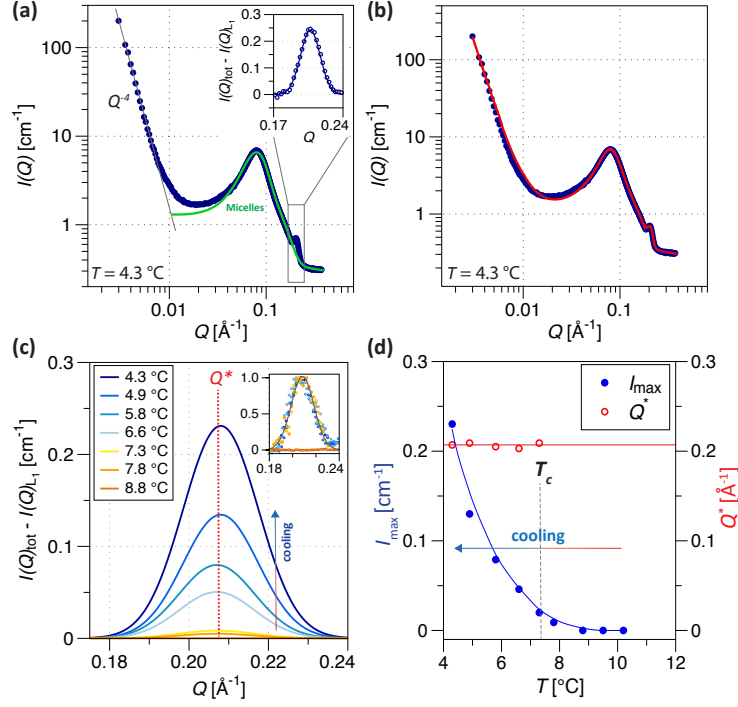
Figure 5: Decomposition of the SANS scattered intensity into the micellar and lamellar contributions. (a) Radially averaged scattered intensity at $T = 4.3$ °C and 15 wt% of NaLAS (full blue circles). A core-shell ellipsoidal model is fitted to the micellar contribution at intermediate-Q (green solid curve). The low-Q and high-Q ranges, associated with the lamellar phase, are fitted with a power law $\propto Q^{-4}$ and a Gaussian profile, respectively. The Gaussian curve is fitted to the data after subtracting the micellar contribution from the scattering intensity, as shown in the inset. (b) Representative fit to the scattered profile by adding the three different components shown in (a). (c,d) The intensity of the high-Q lamellar peak increases with decreasing the temperature, whilst the peak location intensity at $Q^* \approx 0.207$ Å^{-1} remains unchanged. The inset in (c) shows the shape-invariant behavior of the normalized intensity of the lamellar phase high-Q contribution.
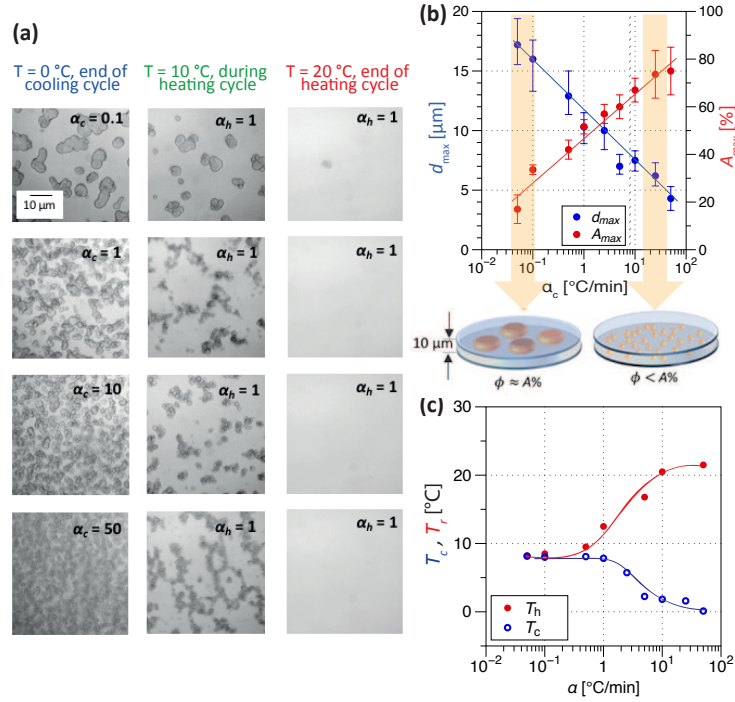
Figure 6: Effect of cooling and heating rates on the growth and dissolution of the MLVs. (a) Different cooling rates ($\alpha_c = 0.1, 1, 10, 50$ °C/min) are investigated for cooling aqueous solutions of 15% NaLAS from 20 °C to 0 °C. During the cooling cycle, smaller droplets at higher number density are formed at higher rates of cooling (left column). A heating ramp at a constant rate of $\alpha_h = 1$ °C/min is applied to all samples, droplets are gradually dissolved back into the solution at around room temperature. Scale bar applies to all micrographs in the panel. (b) Quantitative measurements of the maximum diameter d_{max} of the MLVs and their area coverage A_{max}% obtained by OM at different rates of cooling. In general, the size of the droplets decreases upon increasing the cooling rate α_c, whilst their apparent area coverage increases. (c) The phase transition temperatures for the cooling T_c and the heating T_h cycles are significantly influenced by the rate α, especially for $\alpha > 1$ °C/min.

23
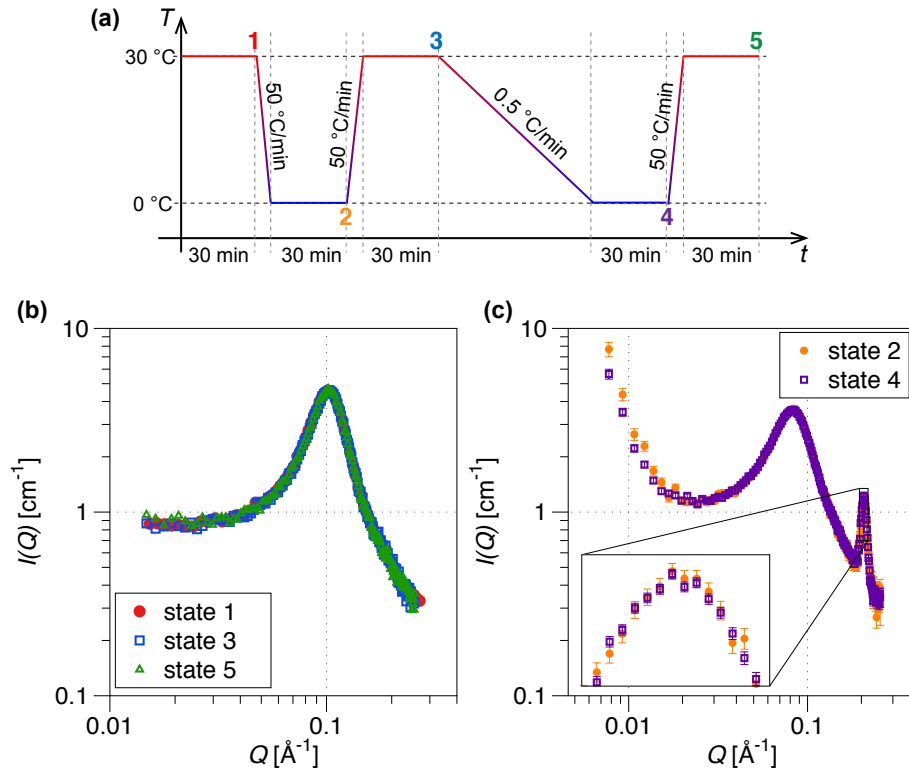
Figure 7: Reversibility and equilibration SANS data of 22.5 % NaLAS solutions subjected to thermal cycling. (a) The temperature profile applied to the NaLAS sample. (b) Identical micellar scattering profiles are obtained regardless of the thermal history applied to the solution, at positions 1, 3, and 5 of the profile shown in (a). (c) Identical micellar profile and Bragg peak, corresponding to a specific mixed micellar and lamellar phase, obtained regardless of the cooling rate. Minor changes in SANS profiles are observed at low-Q range. The states used in the legends of (b) and (c) are identified in the temperature profile shown in (a).
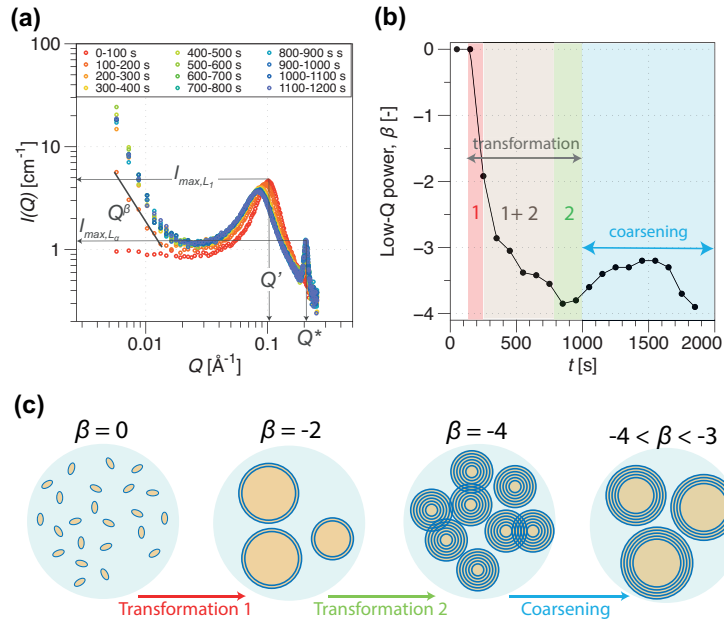
Figure 8: Time-resolved SANS measurements of an aqueous solution of 22.5 % NaLAS, cooled from 30°C to 0°C. (a) Radially averaged SANS data at different time steps, where $t = 0$ corresponds to the time when the sample reaches the final temperature. (b) The evolution of the low-Q power-law in time. The power of the fit changes from $\beta \approx 0$ to $\beta \approx -2$, after a few minutes and then evolves to reach $\beta \approx -4$ associated with compact MLVs. (c) Schematic of the transformations between the micellar and the mixed MLV phase, suggested by the OM and SANS measurements.
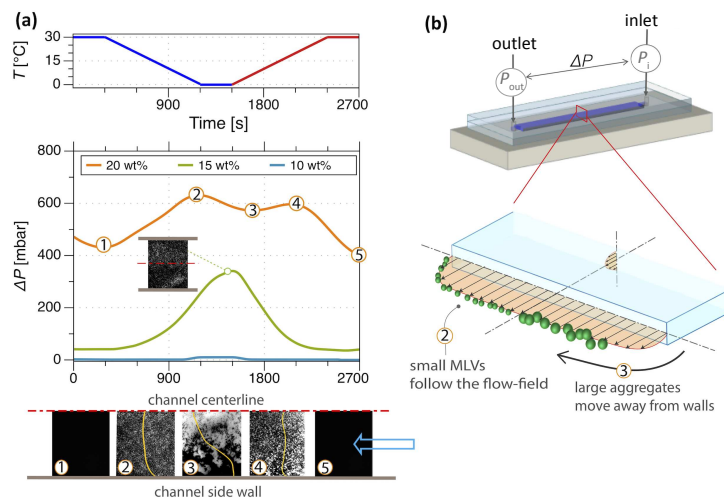
Figure 9: MLVs under flow and pressure drop measurements. (a) A well controlled temperature profile (with $\alpha_c = \alpha_h = 2$ °C/min) is applied to the bottom wall of the microchannel (top). The pressure drop ΔP is used to quantify the effective hydraulic resistance of the different phases of NaLAS solutions flowing at 10 μl/min in the microchannel. Measurements of ΔP are rescaled using the minimum base value obtained obtained for 5% NaLAS concentration. Images show cross-polarised micrographs of the solution under flow at different temperatures and pressures at corresponding circled numbers. Black and white patterns correspond to the micellar and the lamellar phases, respectively. Yellow lines show the distribution of the MLV concentrations from the wall to the center of the channel. (b) Schematic of the microchannel and distribution of MLVs under flow. Small MLVs originally form and homogeneously distribute in the cross-section of the channel. As the number density of droplets increase, their aggregates move towards the center of the channels.

26

[5] R. G. Laughlin, The Aqueous Phase Behavior of surfactants, Academic Press, 1996.

[6] W. R. Hargreaves, D. W. Deamer, Liposomes from ionic, single-chain amphiphiles, Biochem. 17 (18) (1978) 3759–3768.

[7] D. D. Lasic, The mechanism of vesicle formation, Biochem. J. 256 (1) (1988) 1–11.

[8] J. B. Engberts, J. Kevelam, Formation and stability of micelles and vesicles, Curr. Opin. Colloid In. 1 (6) (1996) 779–789.

[9] H. T. Jung, B. Coldren, J. A. Zasadzinski, D. J. Iampietro, E. W. Kaler, The origins of stability of spontaneous vesicles, Proc. Natl.l Acad. Sci. 98 (4) (2001) 1353–1357.

[10] D. E. Discher, A. Eisenberg, Polymer vesicles, Science 297 (5583) (2002) 967–973.

[11] J. Leng, S. U. Egelhaaf, M. E. Cates, Kinetics of the micelle-to-vesicle transition: aqueous lecithin-bile salt mixtures.le-to-vesicle transition: Aqueous lecithin-bile salt mixtures, Biophys. J. 85 (3) (2003) 1624 – 1646.

[12] M. Gradzielski, Vesicles and vesicle gels - structure and dynamics of formation, Journal of Physics: Condensed Matter (19) R655.

[13] C. Richards, G. J. T. Tiddy, S. Casey, Lateral phase separation gives multiple lamellar phases in a "binary" surfactant/water system: The phase behavior of sodium alkyl benzene sulfonate/water mixtures, Langmuir 23 (2) (2007) 467–474.

[14] J. A. Stewart, A. Saiani, A. Bayly, G. J. T. Tiddy, The phase behaviour of lyotropic liquid crystals in linear alkylbenzene sulphonate (las) systems, Colloids Surf A 338 (1) (2009) 155 – 161.

[15] A. S. Poulos, M. Nania, P. Lapham, R. M. Miller, A. J. Smith, H. Tantawy, J. Caragay, J. Gummel, O. Ces, E. S. J. Robles, J. T. Cabral, Microfluidic saxs study of lamellar and multilamellar vesicle phases of linear sodium alkylbenzenesulfonate surfactant with intrinsic isomeric distribution, Langmuir 32 (23) (2016) 5852–5861.

[16] A. Sein, J. B. F. N. Engberts, Micelle to lamellar aggregate transition of an anionic surfactant in dilute aqueous solution induced by alkali metal chloride and tetraalkylammonium chloride salts, Langmuir 11 (2) (1995) 455–465.

[17] M. S. Liaw, M. R. Mackley, J. Bridgwater, G. D. Moggridge, A. E. Bayly, Multilamellar vesicles in a commercial surfactant system, AIChE 49 (11) (2003) 2966–2973.

[18] M. Brooks, G. Moggridge, The effect of additives and the stability of multilamellar vesicles in a commercial surfactant system, Chem. Eng. Res. Des. 84 (2) (2006) 139 – 146.

[19] J. Zipfel, F. Nettesheim, P. Lindner, T. D. Le, U. Olsson, W. Richtering, Cylindrical intermediates in a shear-induced lamellar-to-vesicle transition, EPL 53 (3) (2001) 335.

[20] C. Oliviero, L. Coppola, R. Gianferri, I. Nicotera, U. Olsson, Dynamic phase diagram and onion formation in the system c10e3/d2o, Colloid Surf. A 228 (1) (2003) 85–90.

[21] D. Sato, K. Obara, Y. Kawabata, M. Iwahashi, T. Kato, Re-entrant lamellar/onion transition with varying temperature under shear flow, Langmuir 29 (1) (2013) 121–132.

[22] L. Gentile, M. A. Behrens, L. Porcar, P. Butler, N. J. Wagner, U. Olsson, Multilamellar vesicle formation from a planar lamellar phase under shear flow, Langmuir 30 (28) (2014) 8316–8325, pMID: 24983325.

[23] L. Jia, M.-H. Li, Liquid crystalline polymer vesicles: thermotropic phases in lyotropic structures, Liq. Cryst. 41 (3) (2014) 368–384.

[24] E. Kaler, A. Murthy, B. Rodriguez, J. Zasadzinski, Spontaneous vesicle formation in aqueous mixtures of single-tailed surfactants, Science 245 (4924) (1989) 1371.

[25] Y. Kondo, H. Uchiyama, N. Yoshino, K. Nishiyama, M. Abe, Spontaneous vesicle formation from aqueous solutions of didodecyldimethylammonium bromide and sodium dodecyl sulfate mixtures, Langmuir 11 (7) (1995) 2380–2384.

[26] O. Söderman, K. L. Herrington, E. W. Kaler, D. D. Miller, Transition from micelles to vesicles in aqueous mixtures of anionic and cationic surfactants, Langmuir 13 (21) (1997) 5531–5538.

[27] J. Huang, Y. Zhu, B. Zhu, R. Li, H. Fu, Spontaneous vesicle formation in aqueous mixtures of cationic surfactants and partially hydrolyzed polyacrylamide, J. Colloid Interf. Sci. 236 (2) (2001) 201–207.

[28] L. Zhai, J. Zhang, Q. Shi, W. Chen, M. Zhao, Transition from micelle to vesicle in aqueous mixtures of anionic/zwitterionic surfactants studied by fluorescence, conductivity, and turbidity methods, J. Colloid Interf. Sci. 284 (2) (2005) 698–703.

[29] J. J. Scheibel, The evolution of anionic surfactant technology to meet the requirements of the laundry detergent industry, J. Surfactants Deterg. 7 (4) (2004) 319–328.

[30] A. Pommella, D. Donnarumma, S. Caserta, S. Guido, Dynamic behaviour of multilamellar vesicles under poiseuille flow, Soft Matter 13 (2017) 6304–6313.

[31] O. Arnold, J. C. Bilheux, J. M. Borreguero, A. Buts, S. I. Campbell, L. Chapon, M. Doucet, N. Draper, R. Ferraz Leal, M. A. Gigg, V. E.

Lynch, A. Markvardsen, D. J. Mikkelson, R. L. Mikkelson, R. Miller, K. Palmen, P. Parker, G. Passos, T. G. Perring, P. F. Peterson, S. Ren, M. A. Reuter, A. T. Savici, J. W. Taylor, R. J. Taylor, R. Tolchenov, W. Zhou, J. Zikovsky, Mantiddata analysis and visualization package for neutron scattering andsr experiments, Nuclear Instruments and Methods in Physics Research Section A: Accelerators, Spectrometers, Detectors and Associated Equipment 764 (2014) 156–166.

[32] Y. Xia, G. M. Whitesides, Soft lithography, Angew. Chem. Internatl. 37 (5) (1998) 550–575.

[33] B. Hammouda, Temperature effect on the nanostructure of sds micelles in water, J. Res. NIST 118 (2013) 151–167.

[34] F. Henrich, Small-angle scattering model for multilamellar vesicles, Physical Review E 76 (2007) 051603–1–051603–8.

[35] S. S. Kadam, S. A. Kulkarni, R. C. Ribera, A. I. Stankiewicz, J. H. ter Horst, H. J. Kramer, A new view on the metastable zone width during cooling crystallization, Chem. Eng. Sci. 72 (2012) 10 – 19.

[36] R. M. Miller, O. Ces, N. J. Brooks, E. S. J. Robles, J. T. Cabral, Crystallization of sodium dodecyl sulfate-water micellar solutions under linear cooling, Cryst. Growth Des. 17 (5) (2017) 2428–2437.

[37] C. Huang, D. Quinn, Y. Sadovsky, S. Suresh, K. J. Hsia, Formation and size distribution of self-assembled vesicles, Proc. Natl. Acad. Sci. 114 (11) (2017) 2910–2915.

[38] T. Le, U. Olsson, K. Mortensen, Topological transformation of a surfactant bilayer, Physica B 276-278 (2000) 379 – 380.

[39] A. Shioi, T. A. Hatton, Model for formation and growth of vesicles in mixed anionic/cationic (sos/ctab) surfactant systems, Langmuir 18 (20) (2002) 7341–7348. `doi:10.1021/la020268z`.

[40] T. M. Weiss, T. Narayanan, C. Wolf, M. Gradzielski, P. Panine, S. Finet, W. I. Helsby, Dynamics of the self-assembly of unilamellar vesicles., Phys. Rev. Lett. 94 (3) (2005) 038303.

[41] K. Bressel, M. Muthig, S. Prevost, J. Gummel, T. Narayanan, M. Gradzielski, Shaping vesicles–controlling size and stability by admixture of amphiphilic copolymer, ACS Nano 6 (7) (2012) 5858–5865.

[42] R. Fåhræus, T. Lindqvist, The viscosity of the blood in narow capillary tubes, Am. J. Physiol. 96 (3) (1931) 562–568.

[43] A. Karnis, H. L. Goldsmith, S. G. Mason, Axial migration of particles in poiseuille flow, Nature 200 (1963) 159–160.